Anal. Chem. **2004,** *76,* 7269−7277

Electrokinetically Controlled DNA Hybridization Microfluidic Chip Enabling Rapid Target Analysis

David Erickson,† Xuezhu Liu,‡ Ulrich Krull,‡ and Dongqing Li*,†

Department of Mechanical and Industrial Engineering, University of Toronto, Toronto, Ontario, M5S 3G8, Canada, and Chemical Sensors Group, Department of Chemistry, University of Toronto at Mississauga, Mississauga, Ontario L5L 1C6, Canada

Biosensors and more specifically biochips exploit the interactions between a target analyte and an immobilized biological recognition element to produce a measurable signal. Systems based on surface nucleic acid hybridization, such as microarrays, are particularly attractive due to the high degree of selectivity in the binding interactions. One of the drawbacks of this reaction is the relatively long time required for complete hybridization to occur, which is often the result of diffusion-limited reaction kinetics. In this work, an electrokinetically controlled DNA hybridization microfluidic chip will be introduced. The electrokinetic delivery technique provides the ability to dispense controlled samples of nanoliter volumes directly to the hybridization array (thereby increasing the reaction rate) and rapidly remove nonspecific adsorption, enabling the hybridization, washing, and scanning procedures to be conducted simultaneously. The result is that all processes from sample dispensing to hybridization detection can be completed in as little as 5 min. The chip also demonstrates an efficient hybridization scheme in which the probe saturation level is reached very rapidly as the targets are transported over the immobilized probe site enabling quantitative analysis of the sample concentration. Detection levels as low as 50 pM have been recorded using an epifluorescence microscope.

DNA detection technology plays an important role in almost every field of modern life science and includes applications ranging from drug discovery and development[1] to single-nucleotide polymorphism detection[2−4] to the prevention of bioterrorism.[5,6] One of the most important of these approaches to analysis and diagnostics is hybridization on solid-phase supports, which forms the principle technology behind modern microarrays.[7−12] Hybridization on solid-phase supports exploits the interactions between a target analyte (in this case solution-phase single-stranded DNA, or ssDNA) and an immobilized biological recognition element (a complementary ssDNA probe) to produce a measurable signal (e.g., visual, fluorescent, acoustic, or electrical), which can be interpreted to obtain valuable information regarding the presence of a solution-phase target. The high degree of selectivity for such binding interactions makes nucleic acid hybridization on solid-phase surfaces particularly attractive for development of biosensors and biochips.[13,14]

One drawback of DNA hybridization reactions in microarrays is the relatively long time (often 1−2 h, with many experiments incubated overnight) required for complete hybridization to occur as a result of the diffusion-limited reaction kinetics, making this technology difficult for point-of-care[15] or high-throughput applications.[16] This has led several researchers to investigate the integration of microfluidics-based technologies[17] that are designed to increase the species transfer and therefore kinetic reaction rate and integrate multiple stages of the complete analysis onto a single microscale platform. The use of physical confinement to minimize the distance and time for diffusive transport to the probe sites and therefore enhance the reaction rate is well demonstrated by Cheek et al.,[18] who used a flow-through array of 5−μm-radius channels. Liu et al.[19] introduced a disposable microfluidic device,

* To whom correspondence should be addressed. E-mail: dli@mie.utoronto.ca. Phone: 416-978-1282. Fax: 416-978-7753.

† University of Toronto.

‡ University of Toronto at Mississauga.

(1) Debouck C.; Goodfellow, P. N. *Nat. Genet.* **1999**, *21*, 48−50.
(2) Chen, X.; Sullivan, P. F. *Pharmacogenomics J.* **2003**, *3*, 77−96.
(3) Sachidanandam, R.; Weissman, D.; Schmidt, S. C.; Kakol J. M.; Stein, L. D.; Marth, G.; Sherry, S.; Mullikin, J. C.; Mortimore, B. J.; Willey, D. L.; Hunt, S. E.; Cole, C. G.; Coggill, P. C.; Rice C. M.; Ning, Z. M.; Rogers, J.; Bentley D. R.; Kwok, P. Y.; Mardis, E. R.; Yeh, R. T.; Schultz, B.; Cook, L.; Davenport, R.; Dante, M.; Fulton, L.; Hillier, L.; Waterston, R. H.; McPherson, J. D.; Gilman, B.; Schaffner, S.; Van Etten, W. J.; Reich, D.; Higgins, J.; Daly, M. J.; Blumenstiel, B.; Baldwin, J.; Stange-Thomann, N. S.; Zody, M. C.; Linton, L.; Lander, E. S.; Altshuler, D. *Nature* **2001**, *409*, 928−933.
(4) Altshuler, D.; Pollara, V. J.; Cowles, C. R.; Van Etten, W. J.; Baldwin, J.; Linton, L.; Lander, E. S. *Nature* **2000**, *407*, 513−516.
(5) Espy, M. J.; Cockerill, F. R.; Meyer, R. F.; Bowen, M. D.; Poland, G. A.; Hadfield, T. L.; Smith, T. F. *J. Clin. Microbiol.* **2002**, *40*, 1985−1988.
(6) Belgrader, P.; Young, S.; Yuan, B.; Primeau, M.; Christel, L. A.; Pourahmadi, F.; Northrup, M. A. *Anal. Chem.* **2001**, *73*, 286−289.
(7) Bryant, P. A.; Venter, D.; Robins-Browne, R.; Curtis, N. *Lancet Infect. Dis.* **2004**, *4*, 100−111.
(8) Cao, Y. C.; Jin, R.; Mirkin, C. A. *Science* **2002**, *297*, 1536−1540.
(9) van't Veer, L. J.; Dai, H. Y.; van de Vijver, M. J.; He, Y. D. D.; Hart, A. A. M.; Mao, M.; Peterse, H. L.; van der Kooy, K.; Marton, M. J.; Witteveen, A. T.; Schreiber, G. J.; Kerkhoven, R. M.; Roberts, C.; Linsley, P. S.; Bernards, R.; Friend, S. H. *Nature* **2002**, *415*, 530−536.
(10) Schena, M. *Microarray Analysis*; Wiley-Liss: Hoboken, N.J., 2003.
(11) Ooi, S. L.; Shoemaker D. D.; Boeke J. D. *Science* **2001**, *294*, 2552−2556.
(12) Blohm, D. H.; Guiseppi-Elie, A. *Curr. Opin. Biotechnol.* **2001**, *12*, 41−47.
(13) Jung, A. *Anal. Bioanal. Chem.* **2002**, *372*, 41−42.
(14) Wang, J. *Nucleic Acids Res.* **2000**, *28*, 3011−3016.
(15) Tüdös, A. J.; Besselink, G. A.; Schasfoort, B. M. *Lab Chip* **2001**, *1*, 83−95.
(16) Andersen P. S.; Jespersgaard C.; Vuust J.; Christiansen M.; Larsen L. A. *Hum. Mutat.* **2003**, *21*, 455−465.
(17) Erickson, D.; Li, D. *Anal. Chim. Acta* **2004**, *507*, 11−26.
(18) Cheek, B. J.; Steel A. B.; Torres, M. P.; Yu Y.-Y.; Yang, H. *Anal. Chem.* **2001**, *71*, 5777−5783.

10.1021/ac049396d CCC: $27.50
Published on Web 11/10/2004

fabricated on polycarbonate plastic by CO_2 laser micromachining, which integrated PCR amplification with DNA hybridization onto a "credit card"-sized substrate in which species transport was accomplished via an external syringe pump in combination with a series of on-chip Pluronic valves (also see Yang et al.[20] for sensitivity details). The authors reported that ~1-h incubation time was required to detect the hybridization event. Also from this group, Liu et al.[21] demonstrated hybridization enhancement through the use of cavitation microstreaming where an array of bubbles was acoustically induced to oscillate, resulting in steady, circulating flows and a 5-fold increase in the signal intensity, over a standard diffusion-based array, for a given analysis time. Anderson et al.[22] also presented a polycarbonate-based device for performing chemical amplification, enzymatic reactions, metering and mixing, and hybridization to GeneChip oligonucleotide microarrays. Species transport was accomplished pneumatically, and hydrophobic vents and Mylar/silicon valves (also pneumatically actuated) were integrated into the chip. Lenigk et al.[23] presented an integrated DNA hybridization biochip consisting of a single polycarbonate channel (etched by CO_2 laser) coupled with a Motorola E-sensor chip,[24] which allowed for continuous monitoring of the rate of hybridization at various locations where probe ssDNA had been deposited by spotting. Fan et al.[25] presented a glass microfluidic chip for performing dynamic DNA hybridization on paramagnetic beads, which were incorporated into the device and held in place by an external magnet. Target samples were introduced into the eight-channel structure pneumatically, and integrated heaters enabled denaturation to allow for subsequent samples to also be examined. McQuain et al.[26] demonstrated the effectiveness of chaotic advection in microscale systems by reducing both the analysis time and the maximum signal intensity. Recently Wang et al.[27] coupled universal zip code microarrays into a poly(methyl methacrylate) microfluidic chip. The device was shown to greatly reduce the amount of time required for hybridization (compared with a standard microarray) and was able to detect point mutations in a *K-ras* oncogene at a level of 1 mutant DNA in 10 000 sequences. Noerholm et al.[28] also recently presented a polymeric device containing a 1000-spot array that was compatible with detection based on use of standard florescence scanning equipment. In each of these cases, species transport was accomplished using pressure-driven flow.

Electrokinetic transport[29] offers significant advantages in terms of fluidic control, amenability for miniaturization (as additional device structures such as pumps and valves are unnecessary), and the steep shear gradients near the walls that may provide for an efficient method for removal of nonspecific adsorption (increased surface shear rate is known to decrease surface concentrations of adsorbed species, see Cohen[30] for an example). Some of these advantages have been exploited by bulk solution electrophoresis techniques[31−34] that serve to increase the local target concentration around the probe site, thereby dramatically increasing the reaction rate. One of the other great strengths of electrokinetic manipulation is the precision with which controlled sample volumes can be dispensed. This has led to the development of a number of sample dispensing/injecting techniques[35−43] that are a necessity for quantitative on-chip analysis.

This work introduces an electrokinetically controlled DNA hybridization microfluidic chip. The chip design consists of a poly(dimethylsiloxane) (PDMS) microfluidic system that is bonded to a glass substrate with an immobilized oligonucleotide array. The channel structure is designed to operate with the high-conductivity buffers that are required for efficient hybridization. The electrokinetic control facilitates dispensing of nanoliter sample volumes and rapid removal of nonspecifically adsorbed material. This implementation enables hybridization, washing, and scanning procedures to be conducted simultaneously. The result is that all processes from sample dispensing to detection of hybridization can be completed in as little as 5 min. The rapid and efficient mass transfer allows for rapid equilibration of hybridization and therefore quantitative analysis of the sample concentration. Detection levels as low as 50 pM have been recorded using a standard epifluorescence microscope.

EXPERIMENTAL SECTION

Materials and Reagents. The positive masters used for replica molding of the microfluidic chips were manufactured by exposing SU-8-25 negative photoresist from MicroChem (Newton, MA), followed by development in 4-hydroxy-4-methyl-2-pentanone (Fluka Chemie). The chips were cast in PDMS using a Sylgard

(19) Liu, Y.; Rauch, C. B.; Stevens, R. L.; Lenigk, R.; Yang, J.; Rhine, D. B.; Grodzinski, P. *Anal. Chem.* **2002**, *74*, 3063−3070.
(20) Yang, J.; Liu, Y.; Rauch, C. B.; Stevens, R. L.; Liu, R. H.; Lenigk, R.; Grodzinski, P. *Lab Chip* **2002**, *2*, 179−187.
(21) Liu, R. H.; Lenigk, R.; Druyor-Sanchez, R. L.; Yang, J.; Grodzinski P. *Anal. Chem.* **2003**, *75*, 1911−1917.
(22) Anderson R. C.; Su, X.; Bogdan, G. J.; Fenton, J. *Nucleic Acids Res.* **2000**, *28*, E60.
(23) Lenigk, R.; Liu, R. H.; Athavale, M.; Chen, Z.; Ganser, D.; Yang, J.; Rauch, C.; Liu, Y.; Chan, B.; Yu, H.; Ray, M.; Marrero, R.; Grodzinski, P. *Anal. Biochem.* **2002**, *311*, 40−49.
(24) Umek, R. M.; Lin, S. W.; Vielmetter, J.; Terbrueggen, R. H.; Irvine, B.; Yu, C. J.; Kayyem, J. F.; Yowanto, H.; Blackburn, G. F.; Farkas, D. H.; Chen, Y. P. *J. Mol. Diagn.* **2001**, *3*, 74−84.
(25) Fan, Z. H.; Mangru, S.; Granzow, R.; Heaney, P.; Ho, W.; Dong, Q.; Kumar, R. *Anal. Chem.* **1999**, *71*, 4851−4859.
(26) McQuain, M. K.; Seale, K.; Peek, J.; Fisher, T. S.; Levy, S.; Stremler, M. A.; Haselton, F. R. *Anal. Biochem.* **2004**, *325*, 215−226.
(27) Wang, Y.; Vaidya, B.; Farquar, H. D.; Stryjewski, W.; Hammer, R. P.; McCarley, R. L.; Soper, S. A.; Cheng, Y.-W.; Barany, F. *Anal. Chem.* **2003**, *75*, 1130−1140.
(28) Noerholm, M.; Bruus, H.; Jakobsen, M. H.; Telleman, P.; Ramsing, N. B. *Lab Chip* **2004**, *4*, 28−37.
(29) Santiago J. G. *Anal. Chem.* **2001**, *73*, 2353−2365.
(30) Cohen Y. *Macromolecules* **1988**, *21*, 494.
(31) Edman, C.; Raymond. D.; Wu, D.; Tu, E.; Sosnowski, R.; Butler, W.; Nerenberg, M.; Heller, M. *Nucleic Acids Res.* **1997**, *25*, 4907−4914.
(32) Sosnowski, R. G.; Tu, E.; Butler, W. F.; O'Connel, J. P.; Heller, M. J. *Proc. Natl. Acad. Sci. U.S.A.* **1997**, *94*, 1119−1123.
(33) Raddatz, S.; Mueller-Ibeler, J.; Kluge, J.; Wäss, L.; Burdinski, G.; Havens, J. R.; Onofrey, T. J.; Wang, D.; Schweitzer, M. *Nucleic Acids Res.* **2002**, *30*, 4793−4802.
(34) Syrzycka, M.; Sjoerdsma, M.; Li, P. C. H.; Parameswaran, M.; Syrzycki, M.; Koch, C. A.; Utkhede, R. S. *Anal. Chim. Acta* **2003**, *484*, 1−14.
(35) Fu, L. M.; Yang, R. J.; Lee, G. W. *Anal. Chem.* **2003**, *75*, 1905−1910.
(36) Fu, L. M.; Yang, R. J.; Lee, G. B.; Liu, H. H. *Anal. Chem.* **2002**, *74*, 5084−5091.
(37) Fu, L. M.; Yang, R. J.; Lee, G. B. *J. Sep. Sci.* **2002**, *25*, 996−1010.
(38) Dang, F.; Zhang, L.; Jabasini, M.; Kaji, N.; Baba, Y. *Anal. Chem.* **2003**, *75*, 2433−2439.
(39) Jacobson, S. C.; Ermakov, S. V.; Ramsey, J. M. *Anal. Chem.* **1999**, *71*, 3273−3276.
(40) Harrison, D. J.; Manz, A.; Fan, Z.; Ludi, H.; Widmer, H. M. *Anal. Chem.* **1992**, *64*, 1926−1932.
(41) Jacobson, S. C.; Culbertson, C. T.; Daler, J. E.; Ramsey, J. M. *Anal. Chem.* **1998**, *70*, 3476−3480.
(42) Sinton, D.; Ren, L.; Li, D. *J. Colloid Interface Sci.* **2003**, *266*, 448−456.
(43) Ermakov, S. V.; Jacobson, S. C.; Ramsey, J. M. *Anal. Chem.* **2000**, *72*, 3512−3517.

184 silicone elastomer kit (Dow Corning, Midland, MI). Chemicals used in the (3-glycidoxypropyl)trimethoxysilane (GOPS) surface modification were from Sigma-Aldrich Canada (Oakville, ON, Canada). All oligonucleotide probes were obtained from Integrated DNA Technologies (Coralville, IA). All buffers were made using chemicals from Sigma-Aldrich Canada, were autoclaved, and were prepared with double-distilled water. A solution of 0.5× SSC with 100 mM phosphate buffer (pH 7.0) was used in the on-line experiment and was made by diluting and mixing 20× SSC stock solution (pH 7.0) and 200 mM phosphate buffer (pH 7.0).

Surface Modification and Oligonucleotide Probe Immobilization. Oligonucleotide immobilization on glass slides was done using previously published protocols[44] developed by Maskos and Southern.[45] Briefly, a glass slide (Fisher Finest, 75 mm × 25 mm, 1.0 mm thick) was cleaned with soap and put into water for 30 min of low-power sonication. The slide surface was further sequentially treated with a mixture of 30% hydrogen peroxide, ammonia, and water (v/v, 1:1:5) at 80 °C for 20 min and 30% hydrogen peroxide, hydrochloric acid, and water (v/v, 1:1:5) at 80 °C for 20 min. After cooling, the slide was sequentially washed with distilled water, methanol, dichloromethane, and anhydrous ethyl ether. The slide was kept in an oven of 120 °C before reaction. The above procedure was used for removing contamination, creating surface attachment sites such as hydroxyl groups, and controlling the surface roughness.[46] The treated slide was put into a 500-mL round-bottom flask with 30 mL of GOPS and 1 mL of *N,N*-diisopropylethylamine (Hünig's base) in 100 mL of toluene and was left to reflux overnight. The slide was then washed with methanol, dichloromethane, and anhydrous ethyl ether and was kept in a vacuum desiccator before use. A 15 μM concentration of of the ssDNA probe 5′-NH_2C_{12}-dA_{20} (or 5′-NH_2C_{12}-dA_{20}−Cy5−3′, as a cyanine-based marker for investigation of probe immobilization) in water was then manually applied to the modified glass slide using a pipet tip. The covalent reaction between the epoxy group of GOPS and the amino linker of the oligonucleotide fixed the probe molecules to the surface. The probes were pipetted onto the surface in a specified pattern consistent with the channel structure to be used, resulting in an average probe site diameter of 2 mm. Five such probe site spots were arranged with a center-to-center distance of 5 mm to fit the 30-mm-long hybridization channel of the chip (the chip layout will be described in detail in the following section). After overnight storage in a humid environment, the slides were thoroughly washed with 1× SSC buffer for 10 min and rinsed with water.

Chip Microfabrication and Layout. The microfluidic chips developed for this application were composed of a PDMS upper substrate that contained the microchannel structure and sample ports and a lower glass substrate that served as a substrate for the hybridization array, as shown in Figure 1a. The upper PDMS substrates were microfabricated using a soft lithography/rapid prototyping technique based on that developed by Duffy et al.[47] Briefly, masters containing the desired microchannel pattern, as shown in Figure 1b, were made by spin coating SU-8-25 negative

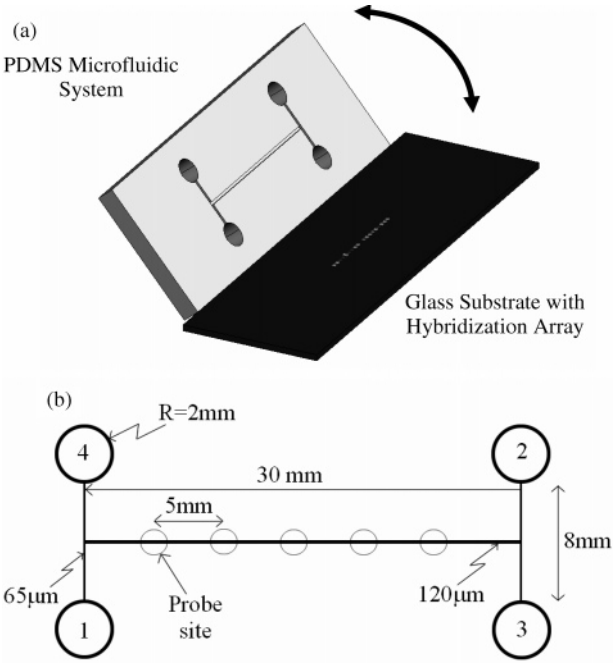

Figure 1. (a) 3D overview of and assembly procedure for PDMS fluidics and immobilized hybridization array. (b) H-type channel structure for DNA hybridization chip: (1) sample port, (2) auxiliary port, (3) buffer port, and (4) wash port.

photoresist on a glass slide at 1800 rpm for 10 s and at 4000 rpm for 40 s, with a ramping phase of 5 s between stages in order to obtain a smooth film with a thickness of 8 μm (corresponding to the eventual channel height). The photoresist film was then hardened by a two-stage direct contact preexposure bake procedure (65 °C for 3 min and 95 °C for 7 min) and exposed to UV radiation (Leitz, 250 W, band-pass filter 325−700 nm) for 1 min through a 3500 dpi transparency mask (UTPress, Toronto, ON, Canada) containing the desired channel pattern designed in AutoCAD. A two-stage postexposure bake procedure (65 °C for 1 min, 95 °C for 2 min) was then used to enhance cross-linking in the exposed portion of the film. The slide was then placed in unstirred 4-hydroxy-4-methyl-2-pentanone developer solution for 3 min to dissolve the unexposed photoresist and finally rinsed in distilled water, leaving a positive relief containing the microchannel pattern.

Liquid PDMS casts were prepared by thoroughly mixing the base and curing agent at a 20:1 ratio. The mixture was then poured over the master and allowed to cure at 65 °C for at least 6 h. This yielded a negative cast of the microchannel pattern in the PDMS slab. Reservoirs were then cut directly into the flexible PDMS using a punch. To form the enclosed chip, the PDMS substrate was plasma treated, aligned, and then placed in direct contact with the glass substrate, such that the 120-μm-wide hybridization channel passed through each of the predeposited probe sites. The oxidizing plasma treatment was conducted by placing the PDMS slab in an air plasma cleaner (PDC-32G, Harrick Scientific, Ossining, NY) for 25 s. Exposure to the plasma for longer than 25 s was found to significantly degrade the seal between the PDMS and the unexposed glass substrate. In general, the alignment was done by manually aligning the fluidic system with landmarks on the underside of the glass substrate, which indicated the location of the hybridization array. By using a PDMS base-

(44) Watterson, J. H.; Piunno, P. A. E.; Krull, U. J. *Anal. Chim. Acta* **2002**, 457, 29−38.
(45) Maskos, U.; Southern E. M. *Nucleic Acids Res.* **1992**, *20*, 1679−1684.
(46) Henke, L.; Nagy, N.; Krull, U. J. *Biosens. Bioelectron.* **2002**, *17*, 547−555.
(47) Duffy, D.; McDonald, J. C.; Schueller, O. J. A.; Whitesides, G. M. *Anal. Chem.* **1998**, *70*, 4974−4984.

to-linker concentration of 20:1 (instead of the recommended 10:1) and by optimization of the plasma exposure time, it was found that the spontaneous seal that was formed between the two substrates could last indefinitely without significant leakage.

The H-type chip layout is shown in Figure 1b. The chip includes one 30-mm-long, 120-μm-wide hybridization channel and two 8-mm-long, 65-μm-wide sidearms leading to four ports for holding buffers and electrodes. The channel height is 8 μm. The dimension of the PDMS pad is 45 mm (L) $\times$ 20 mm (W) $\times$ 5 mm (H), which fits the 75 mm $\times$ 25 mm glass slide used as the substrate for oligonucleotide immobilization.

Instrumentation and Analysis Protocols. Target transport visualization and on-line hybridization detection was conducted using a microfluidics test bench developed at the University of Toronto. Briefly, electrokinetic transport of the oligonucleotides was generated using a high-voltage power source (Spellman High Voltage, Hauppauge, NY) and a custom-built electrical switching board with eight leads each with an independently adjustable output voltage. Cy3-labeled oligonucleotide transport was visualized using a Leica DM-LB fluorescence microscope (Leica Microsystems Canada, Richmond Hill, ON, Canada) with tahe following: a 10$\times$, 0.3 NA long working distance objective, the appropriate filter set (excitation, band-pass 546 nm/12 nm; emission, 600 nm/40 nm band-pass), and a broadband 100-W mercury illumination source. A 12-bit Retiga-1300 cooled digital CCD camera (Qimaging, Burnaby, BC, Canada) was used for imaging and light intensity digitization. Hybridization scanning was also conducted using this optical system with a 32$\times$, 0.6 NA objective, the camera set for 50-ms integration time, maximum binning and 100$\times$ electronic gain, and a Leica DMSTC computer-controlled stage (0.1$-\mu$m resolution, travel speed 5$-$30 000 μm/s) coupled to image acquisition software (Improvision, Guelph, ON, Canada). The scanning program extracted the hybridization channel intensity profile by automatically capturing and storing an image every 5 0μm along the length of the channel. The average intensity of the pixels in a 50 μm by 50 μm square at the middle of the 120-μm-wide channel was then taken as the local point intensity value. In general, a scan of the 30-mm-long hybridization channel required 4 min. For off-line experimentation and quality control of probe/target immobilization/hybridization, a Bio-Rad ChipReader (Hercules, CA) was used to acquire fluorescence images from the glass slides. Cy5- and Cy3-labeled oligonucleotides were used for investigation of the effects of varying the density of immobilized and hybridized oligonucleotides.

After chip assembly, hybridization buffer was pipetted into one of the ports, shown in Figure 1b, and allowed to fill the fluidic system by capillary pressure. Prior to first use, the chips were then flushed using a syringe vacuum for 10 min to remove any contaminants that may have been introduced during microfabrication or assembly. All four ports were then filled with hybridization buffer; the chip was placed into the electrical harness and platinum electrodes, wired to the switching board, were manually inserted into the ports. An electrical check was then conducted to ensure fluidic continuity and to test the integrity of the PDMS/glass seal (a high current load suggested a fluidic leak and therefore failure of the seal). A prescan of the channel was then conducted to obtain the background intensity of the hybridization channel. Buffer in the sample port, typically (1), was then replaced with sample containing the Cy3-labeled probes. A sample plug of known volume was then electrokinetically dispensed and sent to the hybridization array (such that transport, hybridization, and removal of nonspecific adsorption occurred simultaneously) using the procedure outlined in detail in the Electrokinetically Controlled Sample Loading, Dispensing, and Washing section below. Approximately 30 s after the sample plug was dispensed, the hybridization scan was conducted with the images being post-processed by subtracting the prescan image from the final image to obtain the true hybridization intensity profile. After use, the chip was removed from the harness and regenerated by flushing with formamide for 10 min to denature the hybrids followed by a 10-min buffer flush. In general, it was found that the chips could be reused over 10 times without significant loss of signal.

RESULTS AND DISCUSSION

Microfluidic Chip Design and Characterization. The hybrid approach using PDMS/glass enabled the final enclosed chip to be assembled at room temperature, thereby avoiding potential probe damage in the high-temperature bonding process often associated with other microfabrication techniques. This approach also avoided the use of a secondary postassembly immobilization and any need for chip sealing using tape. Additionally, the flexibility in being able to seal the PDMS slab over the probe sites allowed each site to span the width of the hybridization channel. As will be shown, this was a necessary condition for implementation of quantitative analysis of hybridization. PDMS also exhibited very low autofluorescence in the visual range compared to most hard plastics.[48] The speed and low cost with which new chip designs could be manufactured enabled the rapid experimental investigation of several different channel layouts, and the approach and materials that were used are amenable to mass production.

In its simplest form, two transport stages are required for the operation of a DNA hybridization chip: a delivery stage in which the DNA targets are introduced to the probe sites for hybridization, and a subsequent washing stage in which the remaining bulk phase and nonspecifically adsorbed targets are removed in preparation for scanning. The inherent difficulty in designing an electrokinetic transport scheme for such a chip is that traditional DNA transport buffers, used in electrophoresis, such as 1$\times$ TBE, which exhibit relatively high electroosmotic mobility, are incompatible with the hybridization reaction due to the low salt content. High-salt buffers that are compatible with DNA hybridization, such as 1$\times$ SSC or 1$\times$ PBS, must be used despite their poor electrokinetic transport properties. The high conductivity of these hybridization buffers resulted in a high current load when electrokinetic potentials were applied, leading to both significant electrolysis and Joule heating. The electrolysis, coupled with the relatively poor buffering strength of 1$\times$ SSC, led to dramatic changes in local pH, which interfered with the hybridization reaction. To combat this difficulty, a new hybridization buffer was developed consisting of 0.5$\times$ SSC to promote hybridization with an additional 100 mM phosphate buffer to better regulate the pH level in the channel. Experiments revealed that with this buffer the pH value in the channel and sample ports remained stable

(48) Chabinyc, M. L.; Chiu, D. T.; McDonald, J. C.; Stroock, A. D.; Christian, J. F.; Karger, A. M.; Whitesides, G. M. *Anal. Chem.* **2001**, *73*, 4491$-$4498.

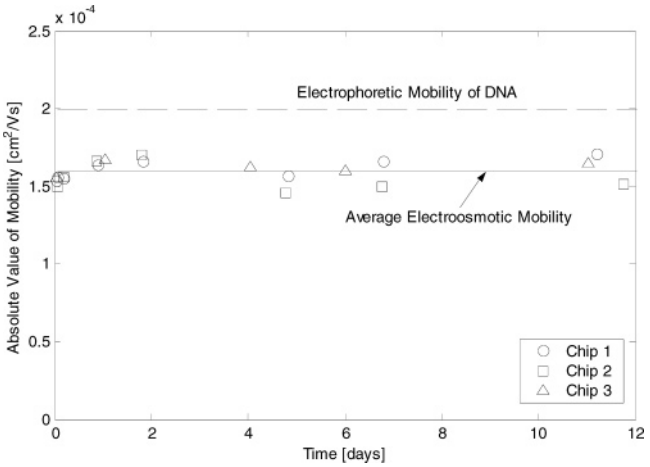

Figure 2. Magnitude of the electroosmotic mobility of the PDMS/glass microfluidic system for 0.5× SSC + 100 mM buffer (pH 7.0) compared with the electrophoretic mobility of dT_{20} DNA targets. Note that since the electroosmotic mobility is negative (average -1.6×10^{-4} cm^2/V·s) the apparent mobility of the DNA targets is $+0.4 \times 10^{-4}$ cm^2/V·s opposite the direction of flow.

for over 30 min when the driving voltages (described in the following section) were applied. When the driving voltages were applied for longer times, slight changes in pH could be detected; however, for the range of experimental times used here (≤60 min), no significant effect on the hybridization reaction or the fluorescence intensity was observed. Standard microarray hybridization experiments have also revealed this buffer to be equivalent to 1× SSC in effectiveness and stabilization of hybridization reactions.

Electrokinetic characterization of the 0.5× SSC + 100 mM phosphate hybridization buffer in the PDMS/glass system was conducted using a series of current monitoring buffer displacement experiments as has been described by others.[49,50] The results of the mobility measurements in three separate chips over the course of 12 days are compared in Figure 2. The average electroosmotic mobility over this time period was -1.6×10^{-4} cm^2/V·s (the negative magnitude implying that flow is directed in the direction opposite to the potential gradient, or from the positive to the negative electrode), and remained stable. The well-known instability in the electroosmotic mobility of PDMS systems[51] was observed when lower conductivity buffers were examined; however, this effect did not appear to be significant here and, as will be shown, the chip design is not sensitive to this effect.

The electrophoretic mobility of the ssDNA targets was measured using a standard cross-dispensing technique[43] and computed by measuring the peak-to-peak displacement over a known period of time, at a well-defined electric field strength. The experiment was repeated in two separate PDMS/glass chips prepared under conditions identical to those described above. The average electrophoretic mobility of the targets was found to be $+2.0 \times 10^{-4}$ cm^2/V·s, and this value is compared to the magnitude ot the electroosmotic mobility for the PDMS/glass system in Figure 2. The summation of the electroosmotic and electrophoretic mobilities yields an apparent mobility of $+0.4 \times 10^{-4}$ cm^2/V·s for the DNA targets in the direction opposite to the bulk flow (or in the direction of increasing applied potential).

Electrokinetically Controlled Sample Loading, Dispensing, and Washing. The fact that the apparent target transport is in the direction opposite to that of the bulk electroosmotic flow complicated the design of the microfluidic system. Since the buffer solution is continuously transported from the upstream (high potential) to the downstream (low potential) reservoir, during the delivery phase the sample port must serve as a waste reservoir for the buffer solution and the buffer port must serve as a waste reservoir for the DNA targets (which as outlined above are transported from the low-potential to the high-potential reservoir). Analogously, during the washing stage, the identical transport conditions exist with the added complication that the undispensed sample must be retracted to the sample port to avoid contamination during hybridization scanning. To meet the demands of this application, an H-type channel structure (see Figure 1b) and two-stage (loading and delivery/washing) counterflow delivery technique was developed.

The applied voltage schemes and time-lapse images of the Cy3-labeled oligonucleotides during these two stages are shown in Figure 3. In the first stage (loading) a sample plug of controlled volume is loaded into the hybridization channel. The volume of the sample plug is controlled by the length of time this stage is held. During this loading stage, the main potential was applied between (1) and (3) with an additional offset voltage applied to port 4 for restriction of the flow into the sidearm leading to this port. Once a sample plug of desired volume had been loaded, the dispensing/washing stage is initiated (in which the sample plug is dispensed and the nonspecific adsorption removed) by switching the voltage scheme such that the main potential was applied between the wash (4) and buffer (3) ports, with an additional voltage applied at (1) to retract the targets in the dispensing arm back to the sample port, ensuring no signal contamination during hybridization scanning (as shown in Figure 3). The fact that the magnitude of the electrophoretic mobility of the DNA exceeded the electroosmotic mobility of the channel enabled the (3) port to continuously supply fresh hybridization buffer while simultaneously acting as the target waste port. In the experiments that are reported herein, 0.5× SSC + 100 mM phosphate buffer (pH 7.0) was used both as a hybridization buffer and as a wash buffer. However, the H-type channel design allowed for a separate wash buffer in the auxiliary port (2) to be used if desired. Since this was not required here, (2) was allowed to float in both stages.

Due to the number of geometric variables in the system (e.g., side and dispensing channel lengths and widths), the sample delivery processes described above and the associated voltage schemes were optimized using numerical simulations conducted with the BLOCS[52,53] finite element code. The results are shown in Figure 4, and the effects of ideal and nonideal voltage adjustment on the sample loading (a) and delivery (b) are demonstrated. Details on the microscale transport phenomena and numerics used here are available in an earlier publication by

(49) Sinton, D.; Escobedo-Canseco, C.; Ren, L.; Li, D. *J. Colloid Interface Sci.* **2002**, *254*, 184−189.
(50) Huang, X.; Gordon, M. J.; Zare, R. N. *Anal. Chem.* **1988**, *60*, 1837−1838.
(51) Ren, X.; Bachman, M.; Sims, C.; Li, G. P.; Allbritton, N. *J. Chromatogr., B* **2001**, *762*, 117−125.
(52) Erickson, D.; Li, D. *Langmuir* **2002**, *18*, 1883−1892.
(53) Biddiss, E.; Erickson, D.; Li, D. *Anal. Chem.* **2004**, *76*, 3208−3213.

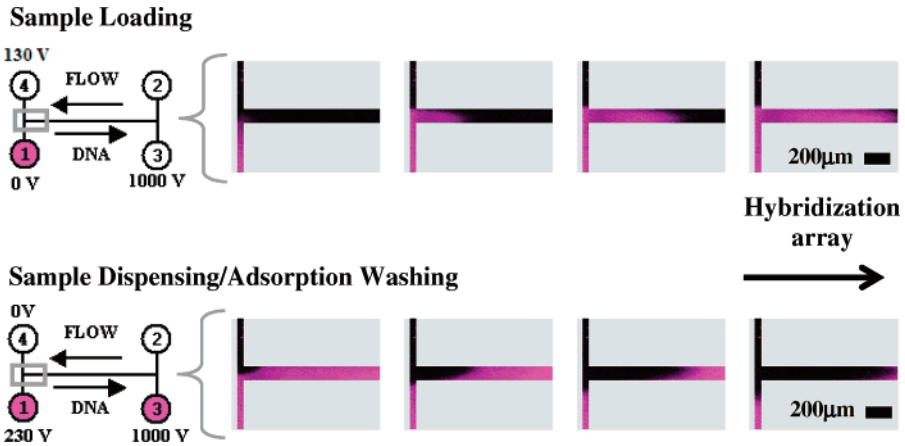

Figure 3. Electrokinetically controlled sample loading and dispensing/washing of DNA targets to the hybridization array. Left images show voltage scheme in each stage while right images show time-lapse pictures of the Cy3-labeled targets at 1-s intervals. In the time-lapse images, the vertical channel is the dispensing arm and the horizontal channel is the hybridization microchannel.

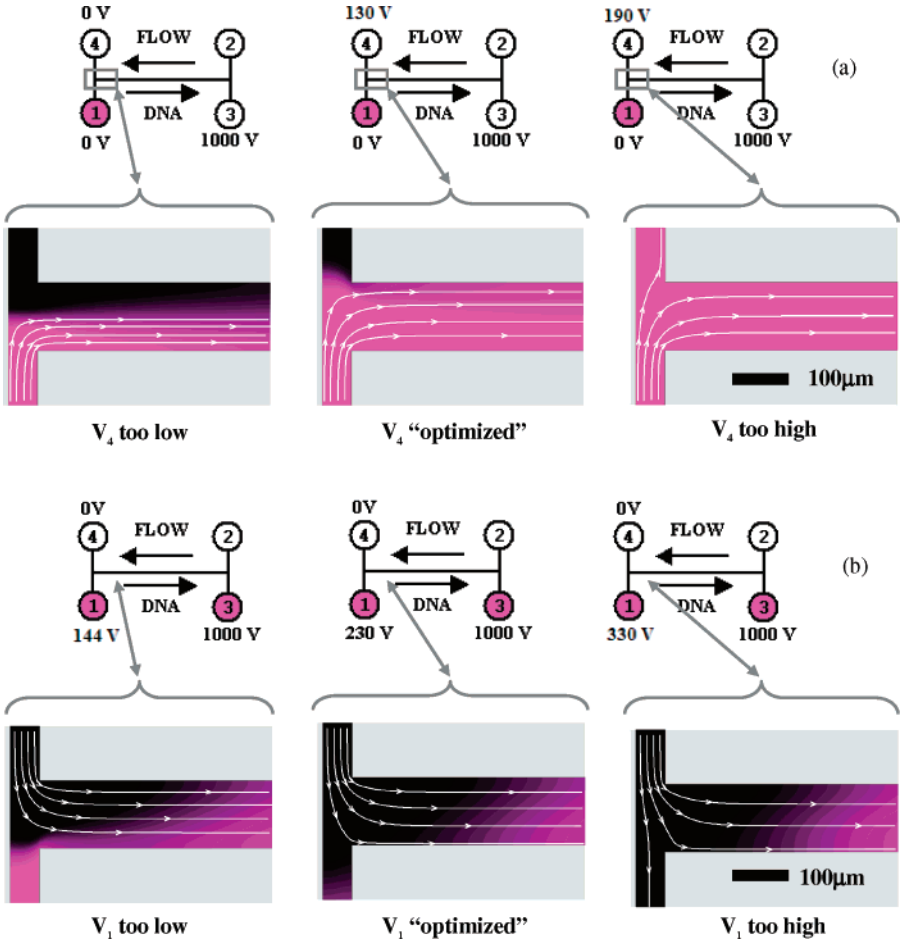

Figure 4. Numerical simulations demonstrating effect of nonoptimized (a) loading and (b) washing/dispensing voltage configuration on operation of DNA chip. Arrows and lines represent streamlines for net electrokinetic transport field (i.e., electroosmosis and electrophoresis) of the targets. As can be seen, when V_4 is too low in the sample loading stage (a) a full sample is not dispensed while too high results in leakage in to the wash buffer reservoir. In the dispensing stage (b), when V_1 is too low leakage occurs from the sample reservoir while too high results in a slower net transport speed. Loading images show steady-state transport while lower images are for 3 s after switching.

Erickson and Li.[54] The lines in these figures are representative of the net electrokinetic transport of the ssDNA targets (i.e., convection and electrophoresis). As can be seen in Figure 4a, during the dispensing phase, the application of a voltage that was too low at the wash reservoir (4) resulted in incomplete sample dispensing. A voltage that was too high resulted in significant sample leakage and flow channel contamination. Figure 4b is the equivalent figure for the washing process demonstrating how a voltage that was too low when applied at the sample reservoir

(54) Erickson, D.; Li, D. In *Biomems and Biomedical Nanotechnology,* Vol. IV: *Biomolecular Sensing, Processing and Analysis*; Bashir, R., Wereley, S., Eds.; Kluwer Academic Publishing: New York, in press.

resulted in leakage into the buffer reservoir. A voltage that was too high resulted in a slightly slower net transport speed. The use of these numerical simulations provided a quick method for examining how changes in the microfluidic layout would affect target transport in the early stages of the chip development and enabled us to find the optimum V_1/V_4 ratio for both the loading and dispensing/washing stages outlined above.

One of the important passive features of the microfluidic device was the minimization of the channel height. This was attempted to the point where further reduction in the channel aspect ratio led to significant sagging and even collapse of the channel structure. A significant advantage of a minimized channel height was that it reduced the vertical diffusive transport distance of the ssDNA targets and therefore increased the frequency of collisions and subsequent probability of hybridization with a complementary probe when passing over the hybridization sites. As will be demonstrated in the following section, this resulted in an extremely fast and efficient hybridization reaction and coupled with the delivery technique described above enabled quantitative analysis of the sample concentration. Reduction of the channel height also minimized the system current load and therefore the associated electrolysis and Joule heating. This was particularly relevant when using high-conductivity buffer and potential field gradients used here (currents on the order of 50 μA were observed for the voltage schemes described above). The heat-transfer properties of a PDMS/glass system are significantly better than those of a pure PDMS/PDMS system;[55] however, it is still possible to reach temperatures near those of the melt temperature of the DNA hybrids that have been used for this work. Operating conditions that resulted in temperatures that were above the melt temperature of the probes would prohibit hybridization. Such operating conditions would not permit effective detection of hybridization, and thus, Joule heating was deemed a major concern for device design and operation. Numerical simulations[55] revealed that for the minimized channel height and voltage schemes outlined above the Joule heating was limited to less than 5 °C above room temperature. To further ensure that this heating was not a problem, the test target−probe complex was selected to be $dA_{20}-dT_{20}$, which has a melt temperature of ~40 °C at the salt concentrations used herein.[56] This hybrid was selected as it provided the lowest possible melt temperature for a 20-mer-length complex and provided the most stringent test of the effect of temperature (i.e., increasing the C−G content would increase the thermal stability of the hybridized dsDNA).

Synchronized On-Line DNA Hybridization, Washing, and Detection. On-line hybridization experiments were conducted by dispensing various volumes of target sample to the hybridization array consisting of five probe sites of 2-mm width that were evenly spaced along a 30-mm length of hybridization channel (see Figure 1b). Initially, the ssDNA targets were concentrated at 500 nM in the 0.5× SSC + 100 mM phosphate buffer. Once the desired volume had been electrokinetically loaded into the hybridization channel, transport of the sample plug through the channel and simultaneous removal of the nonspecific adsorption was initiated by switching to the dispensing/washing voltage scheme (Figure 3). Although nearly 4 min was required to fully transport the sample plug through the hybridization channel, only a short time was required for removal of the nonspecific adsorption. Thus, scanning for hybridization was initiated within ~30 s after the sample plug had been dispensed (the detection scan zone lagged behind the sample plug by roughly 5 mm). The simultaneous removal and transport of the nonspecifically adsorbed targets ensured that this portion of the sample could still become hybridized as it was transported further downstream. The ability to simultaneously complete automatic washing, hybridization, and scanning stages enabled the entire procedure from dispensing to final results to be completed in as little as 5 min (for nanoliter-level sample volumes).

To compare their effectiveness, chip washing experiments were conducted using both the electrokinetic technique described above and an equivalent pressure-driven flow procedure with approximately the same flow velocity. In general, it was found that the pressure-driven washing required 5 times longer than the electrokinetic technique to attain a steady-state adsorption level. Additionally, the steady-state adsorption level for the electrokinetic case was as much as 4 times lower. The speed and efficiency with which the adsorbed materials could be removed was most likely due to the higher surface shear rate, γ, associated with electroosmotic flow than traditional pressure-driven flow. This is suggested by eqs 1a and 1b, as derived from equations found

$$\gamma|_{\mathrm{EO,wall}} = \frac{\mu_{\mathrm{EO}}}{1/\kappa}\nabla\phi \tag{1a}$$

$$\gamma|_{\mathrm{PD,wall}} = \frac{h}{2\mu}\nabla P \tag{1b}$$

in the works of Erickson and Li[57] and Panton,[58] respectively), where μ_{EO} is the electroosmotic mobility, $1/\kappa$ is the double layer thickness, h is the channel height, μ is the viscosity, and $\nabla\phi$ and ∇P are the local potential and pressure field gradients. Assuming a double layer thickness of $1/\kappa = 1$ nm (consistent with the ionic strength of the buffers used herein), and using the measured electroosmotic mobility from Figure 2 and a potential field gradient of 220 V/cm in the hybridization channel, it was calculated that the wall shear rate for the electrokinetic case is 352 000 s^{-1} (calculated using the BLOCS code as mentioned earlier). This would require a pressure drop of 88 000 kPa/m along the hybridization channel as determined from eq 1b, or a velocity of 700 mm/s, which is much larger than the 1 mm/s typically obtainable in microfluidic systems. From eq 1b it is apparent that increasing the channel height can increase the pressure-driven flow shear rate. However, this would be detrimental to hybridization efficiency as will be demonstrated later on in this section. The plug flow associated with electrokinetic transport can also in general serve to reduce the effective size of the depletion zone over the probe sites, as targets are transported into the reaction zone near the surface at the effective transport speed as opposed to parabolic flow where vertical diffusive transport of targets from the center of the channel must be more heavily relied upon.

In addition to affecting the removal rate of adsorbed species, it is also possible that the superposition of the double layer field,

(55) Erickson, D.; Sinton, D.; Li, D. *Lab Chip* **2003**, *3*, 141−149.
(56) Melt temperature data provided by the supplier.
(57) Erickson, D.; Li, D. *J. Colloid Interface Sci.* **2000**, *232*, 186−197.
(58) Panton, R. *Incompressible Flow,* 2nd ed.; John Wiley & Sons: New York, 1996.

applied potential field, Joule heating-induced temperature field, and high-shear rate flow field within the surface bound hybridization array can significantly affect the stability of the target−probe complex. In general, caution was taken here, as outlined above with regard to Joule heating, to minimize these effects. Preliminary experiments at higher voltages, however, have revealed that the coupling of these phenomena within the double layer can be exploited to induce controlled denaturing of the hybrid.[59] The buildup of negatively charged DNA on the surface as the hybridization reaction progresses will increase the local surface charge density. This will likely result in localized increases to the flow/shear rate (as the electroosmotic body force is increased), potentially further enhancing localized mixing. While not exclusively relevant to reactions involving electrokinetics, this may also result in a significant slowing of the expected hybridization reaction rate due to the increased electrostatic repulsion as discussed by Vainrub and Pettitt.[60,61] This may explain why previous hybridization models that do not account for this effect[62] tend to overpredict the reaction rate at points near completion of the reaction.

The results of these experiments for 120-, 35-, and 20-s dispensing times (corresponding to 16.7-, 4.9-, and 2.8-nL sample volumes) are shown in Figure 5 (a−c). The sample volumes were determined by multiplying the channel cross-sectional area (120 μm wide × 8 μm tall = 960 μm^2) by the dispensing time and the measured net transport speed (145 μm/s) in the hybridization channel. Note that the dispensed sample volumes were significantly lower than the total channel volume (28.8 nL). As can be seen in Figure 5, the 16.7- (a) and 4.9-nL (b) samples produced nearly identical results, and each of the five probe sites could be clearly identified. This suggested that a volume of 4.9 nL was approximately the sample size that was required for complete hybridization of the probe sites. For the 2.8-nL sample (c), however, only the first two probe sites could be fully detected and the third was only partially hybridized. The observation of similar fluorescence intensity levels in the first two sites and for half of the third site suggested that target delivery and subsequent hybridization was highly efficient (i.e., the front of the dispensed sample became nearly immediately hybridized upon passing over a compatible probe site until such time as the plug was completely depleted). This was confirmed by the observation that in the latter case no significant fluorescence signal could be detected at the downstream end of the device during either the loading or dispensing/washing stages. The reason for the high efficiency of hybridization was that the relatively small channel height (8 μm) confined the target molecules to be in proximity to the hybridization probes, thereby reducing the vertical diffusive transport distance and increasing the number of target−probe collisions, thereby increasing the probability of hybridization. As mentioned above, reasonably high sample concentrations, 500 nM, were used here when compared with those traditionally encountered in standard microarray experiments. In general, this was done as it represents a "worst-case" scenario since, as is shown above, even these highly concentrated sample plugs can become fully depleted as they pass over a compatible probe site. The highly concentrated samples also provide the most stringent test for adsorption removal using the electrokinetic technique. In general, however, the above demonstrates that the actual amount of DNA required is quite small (2.45 fmol for the saturation case) as the highly efficient kinetics ensure that every target comes in contact with every probe site, as opposed to standard microarray experiments, where a particular target may or may not come in contact with a given probe site.

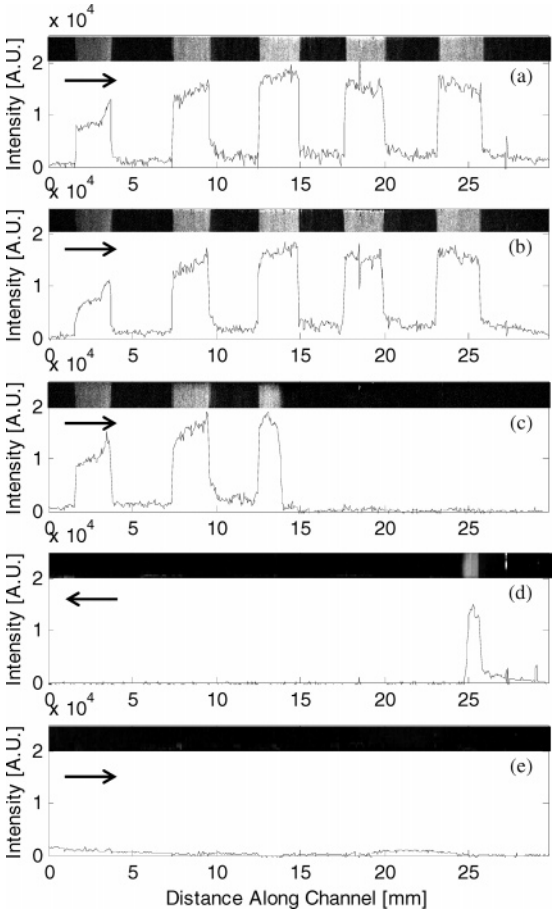

Figure 5. Results of on-line hybridization experiments for (a) 16.7-nL dispensed sample volume (120-s dispensing time), (b) 4.9-nL dispensed sample volume (35-s dispensing time), and (c) 2.8-nL dispensed sample volume (20-s dispensing time) all at 500 nM (all transport from right to left), (d) 4.9-nL dispensed sample (from left to right) at 50 nM, and (e) 16.7-nL sample of noncomplementary DNA at 500 nM dispensed from right to left. Arrows show sample transport direction.

The effect of sample concentration is demonstrated in Figure 5d, where a 50 nM sample of 4.9-nL volume, equivalent to that for Figure 5b, has been dispensed. In this case, the sample was dispensed from the right end of the chip and transported to the left in order to demonstrate that the effect was not directionally biased. Approximately half of the first probe site became hybridized, representing ~1/10th of the total hybridization area as would have been expected as 1/10th the total amount of DNA was transported into the hybridization array. Detection levels here were limited by the use of a standard fluorescence microscope as the detector; however, concentration levels as low as 50 pM were examined by increasing the dispensed sample size to 460 nL. Though the hybridization kinetics were still equivalently fast

(59) Erickson, D.; Liu, X.; Venditti, R.; Krull, U.; Li, D. *Proceedings of the 2004 IMECE,* Anaheim, CA, 2004; IMECE2004-59320.
(60) Vainrub, A.; Pettitt, B. *Chem. Phys. Lett.* **2000**, *323*, 160−166.
(61) Vainrub, A.; Pettitt, B. *Phys. Rev. E* **2002**, *66*, 041905.
(62) Erickson, D.; Li, D.; Krull, U. J. *Anal. Biochem.* **2003**, *317*, 186−200.

to those described above, the longer dispensing time required to transport the femtomole level of target required for detection to the hybridization array increased the total analysis time to 60 min.

Figure 5e shows the results for a 500 nM, 4.9-nL noncomplementary target sample (5′-AAA CAA TCA ATC CGT CGC GG-Cy3−3′). The lack of signal in this case demonstrated that the signals observed in Figure 5a−d were indeed due to specific hybridization as opposed to nonspecific adsorption of the targets.

In Figure 5a−d, we observed that the intensity of fluorescence from spots reached similar levels, but fewer spots became fluorescent when the volume or concentration of the dispensed sample was reduced. Effectively, all of the target oligonucleotides that passed through the hybridization area could be "captured" by the immobilized oligo in a very short period. To further examine the rapid depletion of the sample plug observed in Figure 5c and d, a Peclet number analysis on the vertical diffusion of the targets in the system can be performed. The required downstream length for a target to diffuse from the top of the microfluidic channel to the probe site is given by eq 2,

$$L_{\text{diff}} = (UH/D)H = Pe_{\text{H}}H \qquad (2)$$

where U is the transport velocity, D is the diffusion coefficient, and H is the channel height. Using a diffusion coefficient of 1.3 $\times$ 10^{-10} m^2/s,[62] the channel height of 8 μm, and the 145 μm/s transport speed, the maximum downstream transport distance is L_{diff} = 70 μm, much smaller than the width of the probe sites used herein. Although not fully characterized here, also likely to enhance the reaction rate is the hydrodynamic lift force on the targets caused by the in-channel velocity gradient (as the glass surface exhibits a locally higher electroosmotic mobility than the PDMS component). As described by Zheng et al.[63] and recently observed by Zheng and Yeung[64] in similar PDMS/glass chips, this velocity gradient tends to focus DNA near the bottom of the channel. This would reduce the effective H in eq 2 and thereby further decrease L_{diff}. Only 14 s was required for the oligonucleotides to pass over each probe site, therefore demonstrating that the mass transfer rate observed here was much faster than that seen using conventional microarrays. This highly efficient hybridization using electrokinetic transport provides the potential for quantitative analysis of the target DNA as the concentration of targets can be estimated according to the density of immobilized oligonucleotides (i.e., the saturation concentration) and the volume of the sample plug. Such quantitative analysis is possible based on either calibration of fluorescence intensity (as will be described in the following section) or the number of sequential spots that developed fluorescence intensity signals (in this case, smaller spot widths should be used to increase the overall accuracy). The other major advantage of the rapid hybridization reaction is that it has the potential to enable much lower detection limits. Hybridized targets are concentrated at the first complementary probe site so long as the probe molecules are not saturated.

Off-Line Hybridization on Glass Slides for Density Study. Off-line experiments were done to investigate the effects of oligonucleotide density of the immobilized and hybridized DNA. These data provided quantitative information about the amounts of DNA that were immobilized and that hybridized and were then used to calibrate the dynamic course of the on-line hybridization in a channel. Two series of Cy5-labeled and Cy3-labeled oligonucleotide spots were prepared by directly depositing a known volume and concentration of oligonucleotide solution (concentration series from 1 nM to 1 μM). Comparison of the intensity of the fluorescence signals of immobilized/hybridized oligonucleotides with those of the calibration series provided a basis for estimation of the extent of hybridization on the glass surfaces. By this method, the immobilized/hybridized oligonucleotide densities were estimated to be (1−5) $\times$ 10^{-15} mol/mm^2, which was correspondent with ~20 nm center-to-center molecular spacing on the glass surface. The 2.8-nL, 500 nM sample volume (see Figure 5c) was correspondent to 1.4 $\times$ 10^{-15} mol. The amount of immobilized oligonucleotide on every spot was ~5 $\times$ 10^{-16}−1 $\times$ 10^{-15} mol, which was in the same range as that in the 2.8-nL dispensed sample. As such, almost all the immobilized oligonucleotides could be hybridized by the target when the target was available in molar excess. In the on-line hybridization experiments, it was observed that the immobilized oligonucleotide spots were sequentially saturated as the amount of target was increased. Different target concentrations could be determined simply by counting the number of immobilized spots that were saturated in terms of fluorescence signal.

CONCLUSIONS

In this work, we have introduced the development of an electrokinetically controlled microfluidic chip for DNA hybridization. The design consisted of an H-type channel structure in a PDMS chip, which was bonded to a glass slide containing immobilized single-stranded oligonucleotide probes. The channel structure was developed to operate with the high-conductivity, low-electroosmotic mobility buffers that are required for efficient hybridization reactions. Electrokinetic control allowed for the dispensing of nanoliter target sample volumes and rapid removal of nonspecifically adsorbed material. Hybridization, washing, and scanning procedures were conducted simultaneously, resulting in all processes from sample dispensing to hybridization detection being completed in as little as 5 min. The rapid and efficient mass transfer allowed for rapid equilibration of hybridization and for quantitative analysis of the sample concentration. With extra effort and quality control, it would be possible to improve quantitative determination of target concentrations by decreasing the size and therefore increasing the number of probe sites (it is possible to prepare relatively uniform spots containing immobilized oligonucleotides with 20-nm center-to-center distances). Because of the fast mass transfer between the surface and the bulk solution, the electrokinetically controlled hybridization chip may provide a platform for study of the kinetics of hybridization.

ACKNOWLEDGMENT

We are grateful to the Natural Sciences and Engineering Research Council of Canada for support of this research work. D.E. also acknowledges the financial support of Glynn Williams through a scholarship.

Received for review April 22, 2004. Accepted September 27, 2004.

AC049396D

(63) Zheng, J.; Li H.-W.; Yeung, E. S. *J. Phys Chem.* **2004**, *108*, 10357−10362.
(64) Zheng, J.; Yeung, E. S. *Anal. Chem.* **2003**, *75*, 3675−3680.